Int. J. Heat Mass Transfer. Vol. 34, No. 3, pp. 711–721, 1991
Printed in Great Britain

0017–9310/91 $3.00+0.00

A near wall k–ε formulation for high Prandtl number heat transfer

J. HERRERO, F. X. GRAU, J. GRIFOLL and FRANCESC GIRALT
Departament d'Enginyeria Química i Bioquímica, Divisió VII, Universitat de Barcelona, 43005 Tarragona, Catalunya, Spain

(*Received* 20 *January* 1989 *and in revised form* 29 *January* 1990)

Abstract—An improved form of the so-called 'near-wall' $k-\varepsilon$ turbulence model is proposed. The damping functions accounting for viscous effects at low Reynolds numbers are modified to yield a turbulent viscosity that properly predicts heat transfer rates over a wide range of Prandtl numbers, using a constant turbulent Prandtl number $Pr_t = 0.9$. These modifications aimed at improving the prediction of wall fluxes, also yield a better description of mean velocity and temperature profiles as well as of mean turbulent properties.

INTRODUCTION

THE TWO-EQUATION k–ε model of turbulence has been widely used in numerical simulations due to its simplicity and, to some extent, capability for predicting turbulent flows. For wall-bounded flows, the model has been modified in the past to include turbulence decay near solid boundaries as the Reynolds number decreases. This so-called 'near-wall' k–ε model uses damping functions instead of the empirical constants appearing in the original high Reynolds number formulation [1], in order to account for viscous effects. The use of near-wall models avoids the use of empirical 'laws of the wall' for each different flow studied.

Near-wall models were first postulated by Jones and Launder in 1973 [2, 3]. Several alternative forms have since been published [4–11]. These proposals give, in general, fairly good predictions of turbulent mean properties such as velocity, turbulent kinetic energy and its dissipation rate. However, the model presents some structural deficiencies or drawbacks: (i) it is based on a turbulent viscosity and, thus, implies the identity of normal stresses predicted under the absence of mean normal strain [12] and (ii) the equation for the ε-transport has been established by simply reproducing the structure of the k-transport equation [13]. These limitations become apparent when the model is applied to three-dimensional or even to some two-dimensional flows with complex geometry [14–16]. Despite these deficiencies, k–ε models still remain among the most widely used approaches by engineers and scientists for the solution of practical problems [12].

Other limitations arise when k–ε models are applied to heat and mass transfer calculations at solid boundaries. In these situations they can yield unrealistic predictions for the flux of energy and matter, as well as for the profiles of the corresponding scalar quantities. Existing near-wall formulations yield reasonable predictions for friction factors and, thus, for heat transfer rates when the Prandtl number is of the order of unity, but fail at large Prandtl numbers. For example, the model of Jones and Launder [3], which is one of the best reported in the literature for heat transfer calculations, predicts Nusselt numbers 25% above experimental values for pipe flow at $Pr = 1000$. Under these conditions of low thermal diffusivity, ν_t values very near the wall have a great effect on heat transfer rates. In fact, any model giving small enough ν_t values near the wall, i.e. for $y^+ < 5$, will correctly predict momentum transfer within this region. However, it will not yield realistic heat and mass transfer predictions for high Prandtl numbers if the ν_t profile, in conjunction with a turbulent Prandtl number, has not been modelled properly close to the wall.

In the present work, the near-wall k–ε model proposed by Lam and Bremhorst [10] is adapted to describe both the momentum and heat transfer processes over a wide range of Reynolds and Prandtl numbers. Since there is a large amount of momentum and heat/mass transfer experimental data available in the literature for fully developed pipe and duct flows, a computer simulation of the transfer processes in such systems is used to check the performance of the present and past models.

THEORY

Governing equations

The mean flow is governed by the Reynolds equations which can be written, under the Boussinesq assumption [17], as

$$\frac{\partial U_i}{\partial t} + U_j \frac{\partial U_i}{\partial x_j} = -\frac{1}{\rho}\frac{\partial \Pi}{\partial x_i} + \frac{\partial}{\partial x_j}\left[(\nu + \nu_t)\frac{\partial U_i}{\partial x_j}\right]. \quad (1)$$

In the k–ε approach, the eddy viscosity is modelled as

$$\nu_t = C_D f_\mu \frac{k^2}{\varepsilon} \quad (2)$$

NOMENCLATURE

a, b, c	constants in equation (11)
C_1, C_2, C_m	constants in equations (2) and (4)
C_p	specific heat capacity [J kg^{-1} K^{-1}]
d	constant in equation (12)
E	extra term appearing in equation (4)
f_1, f_2, f_m	damping functions in equations (2) and (4)
h	heat transfer coefficient [W m^{-2} K^{-1}]
k	turbulent kinetic energy [m^2 s^{-2}]
K	thermal conductivity [W m^{-1} K^{-1}]
Nu	Nusselt number, $2Rh/K$
Pr	Prandtl number, ν/α
Pr_t	turbulent Prandtl number
q_w	wall heat flow rate [W m^{-2}]
R	pipe radius or half width of channel [m]
Re	Reynolds number, based on average velocity and diameter
R_k, R_t	turbulent Reynolds numbers, $y\sqrt{k}/\nu$ and $k^2/\nu\varepsilon$, respectively
t	time [s]
T	temperature [K]
T^+	dimensionless temperature, $(T-T_w)/T_*$
T_w	temperature at the wall [K]
T_*	friction temperature, $q_w/\rho C_p u_*$ [K]
U	mean velocity [m s^{-1}]
U^+	dimensionless velocity, U/u_*
u_*	friction velocity [m s^{-1}]
x	axial coordinate [m]
y	normal distance to the wall [m]
y^+	dimensionless distance from the wall, yu_*/ν.

Greek symbols

α	thermal diffusivity [m^2 s^{-1}]
α_t	eddy thermal diffusivity [m^2 s^{-1}]
$\varepsilon, \tilde{\varepsilon}$	dissipation rate of the turbulent kinetic energy, $\varepsilon = \tilde{\varepsilon}+\phi$ [m^2 s^{-3}]
ν	kinematic viscosity [m^2 s^{-1}]
ν_t	kinematic eddy viscosity [m^2 s^{-1}]
Π	combined pressure appearing in equation (1), $P+2/3k\rho$ [Pa]
ρ	density [kg m^{-3}]
$\sigma_k, \sigma_\varepsilon$	empirical constants appearing in equations (3) and (4)
ϕ	term resulting from the ε splitting [m^2 s^{-3}]
ψ	stream function [m^2 s^{-1}]
ω	mean vorticity [s^{-1}].

where the mean turbulent kinetic energy and its dissipation rate are evaluated from differential transport equations

$$\frac{\partial k}{\partial t}+U_j\frac{\partial k}{\partial x_j}=\frac{\partial}{\partial x_j}\left[\left(\nu+\frac{\nu_t}{\sigma_k}\right)\frac{\partial k}{\partial x_j}\right]+\nu_t\left(\frac{\partial U_i}{\partial x_j}+\frac{\partial U_j}{\partial x_i}\right)\frac{\partial U_i}{\partial x_j}-\tilde{\varepsilon}-\phi \quad (3)$$

and

$$\frac{\partial \tilde{\varepsilon}}{\partial t}+U_j\frac{\partial \tilde{\varepsilon}}{\partial x_j}=\frac{\partial}{\partial x_j}\left[\left(\nu+\frac{\nu_t}{\sigma_\varepsilon}\right)\frac{\partial \tilde{\varepsilon}}{\partial x_j}\right]+\nu_t C_1 f_1\frac{\tilde{\varepsilon}}{k}\left(\frac{\partial U_i}{\partial x_j}+\frac{\partial U_j}{\partial x_i}\right)\frac{\partial U_i}{\partial x_j}-C_2 f_2\frac{\tilde{\varepsilon}^2}{k}+E. \quad (4)$$

The σ_k, σ_ε, C_μ, C_1 and C_2 are empirical constants and f_1, f_2, f_μ are damping functions for the near-wall formulation. As in ref. [18], Table 1 summarizes several proposals for these constants and damping functions. The k equation (3) includes the term ϕ, $\varepsilon = \tilde{\varepsilon}+\phi$, which has been introduced by several authors [3–8, 11] to impose the boundary condition $\tilde{\varepsilon} = 0$ at the wall. Otherwise, when $\phi = 0$, ε_w has to be calculated according to the proposals included in Table 1. The extra term E seems to be necessary only when f_1 is taken equal to unity in the near-wall formulation [2, 3]. Table 1 also includes several proposals for E.

The thermal field is governed by the conservation equation

$$U_j\frac{\partial T}{\partial x_j}=\frac{\partial}{\partial x_j}\left[(\alpha+\alpha_t)\frac{\partial T}{\partial x_j}\right] \quad (5)$$

when constant thermal properties are considered.

Numerical scheme

In the present work, the numerical prediction of the velocity field was accomplished using the mean vorticity–stream function formulation. The resulting set of coupled differential equations for fully developed pipe and channel flows was solved using a second-order central finite difference scheme, with a fictitious temporal evolution, and a doubly-coupled ω/ψ and k/ε solver [19].

The enthalpy conservation equation (5) was solved separately from the dynamic field [20] assuming $Pr_t = 0.9$, as suggested by Jones and Launder [3]. The axial thermal diffusion was neglected. A minimum of 250 transverse grid points were used and distances from the wall not larger than $y^+ = 0.5$ covered. Three different regions were distinguished in the generation of the computation mesh. A regularly distributed grid with at least 40 points was used over $0 \leqslant y^+ \leqslant 20$. Beyond $y^+ = 20$ the grid size was linearly increased with a factor not greater than 1.05, until an increment of $\Delta y^+ \approx 10$ was reached. From this location up to the centreline the mesh was kept regular again. With

Table 1. Constants and functions for the k–ε group of models

Proposal	ε_w	C_μ	C_1	C_2	σ_k	σ_ε	f_μ	f_1	f_2	ϕ	E
High Re [1]	Wall function	0.09	1.44	1.92	1.0	1.3	1.0	1.0	1.0	0	0
Jones–Launder [3]	0	0.09	1.45	2.0	1.0	1.3	$\exp[-2.5/(1+R_t/50)]$	1.0	$1-0.3\exp(-R_t^2)$	$2\nu(\partial\sqrt{k}/\partial y)^2$	$2\nu\nu_t(\partial^2 u/\partial y^2)^2$
Hassid–Poreh [4]	0	0.09	1.45	2.0	1.0	1.3	$1-\exp(-0.015R_t)$	1.0	$1-0.3\exp(-R_t^2)$	$2\nu k/y^2$	$-2\nu(\partial\sqrt{\varepsilon}/\partial y)^2$
Hoffman [5]	0	0.09	1.81	2.0	2.0	3.0	$\exp[-1.75/(1+R_t/50)]$	1.0	$1-0.3\exp(-R_t^2)$	$(\nu/y)\,\partial k/\partial y$	0
Launder–Sharma [6]	0	0.09	1.44	1.92	1.0	1.3	$\exp[-3.4/((1+R_t/50)^2)]$	1.0	$1-0.3\exp(-R_t^2)$	$2\nu(\partial\sqrt{k}/\partial y)2$	$2\nu\nu_t(\partial^2 u/\partial y^2)^2$
Dutoya Michard [7]	0	0.09	1.35	2.0	0.9	0.95	$1-0.86\exp[-(R_t/600)^2]$	$1-0.04[-(R_t/50)^2]$	$1-0.3\exp[-(R_t/50)^2]$	$2\nu(\partial\sqrt{k}/\partial y)^2$	$-C_2 f_2\varepsilon\phi/k$
Chien [8]	0	0.09	1.35	1.8	1.0	1.3	$1-\exp(-0.0115y^+)$	1.0	$1-0.22\exp[-(R_t/6)^2]$	$2\nu k/y^2$	$-2(\varepsilon\nu/y^2)\exp(-0.5y^+)$
Reynolds [9]	$\nu\partial^2 k/\partial y^2$	0.084	1.0	1.83	1.09	1.3	$1-\exp(-0.0198R_k)$	1.0	$\{1-0.3\exp[-(R_t/3)^2]\}f_\mu$	0	0
Lam Bremhorst [10]	$\nu\partial^2 k/\partial y^2$	0.09	1.44	1.92	1.0	1.3	$[1-\exp(-0.0165R_k)]^2\times(1+20.5/R_t)$	$1+(0.05/f_\mu)^3$	$1-\exp(-R_t^2)$	0	0
Nagano Hishida [11]	0	0.09	1.45	1.9	1.0	1.3	$[1-\exp(-y^+/26.5)]$	1.0	$1-0.3\exp(-R_t^2)$	$2\nu(\partial\sqrt{k}/\partial y)^2$	$\nu\nu_t(1-f_\mu)(\partial^2 u/\partial y^2)^2$
Present work	$\partial\varepsilon/\partial y=0$	0.09	1.44	1.92	1.0	1.3	$[1-\exp(-0.0066R_k)]^2\times[1+500\exp(-0.0055R_k)/R_t]$	$1+(0.05/f_\mu)^2$	$1-(0.3/D)\exp(-R_t^2)$ $D=1-0.7\exp(-R_k)$	0	0

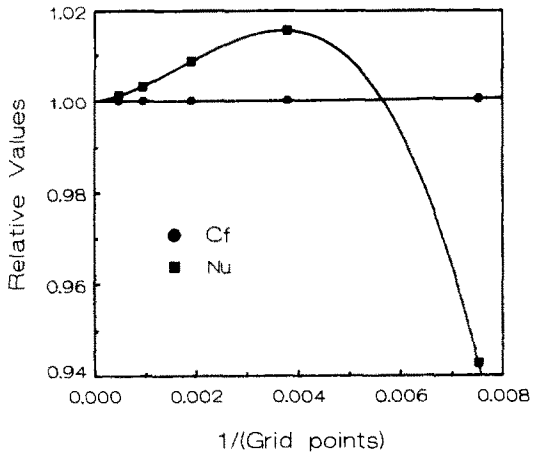

FIG. 1. Effect of grid density on the predicted skin friction coefficients and Nusselt numbers.

this distribution, at least one computational grid point was placed within the linear dimensionless temperature profile region, even for Prandtl numbers as high as 1000.

The effect of grid density on friction factors and Nusselt number predictions is shown in Fig. 1 for five different cases, all at $Re = 40\,000$ and $Pr = 1000$. This figure shows the ratio of predicted to extrapolated values at infinite grid density as a function of the inverse of the number of nodes. The five grids were progressively refined by duplicating the number of points. It is evident that the friction factor is not sensitive to mesh refinement while the Nusselt number predictions for $Pr = 1000$ require, at least, the use of a 250 point grid. It is worthwhile to note that the coarser grid, which leads to a poor prediction of the heat transfer phenomena, locates the first node at $y^+ \approx 1.0$.

The above numerical implementation was used to model the damping functions appearing in equations (2) and (4) and to further compare predictions with previous proposals and experimental data. Table 1 shows the functions and the values of the constants reported by different authors to yield best results when used in equations (2)–(4). Recent reviews on turbulence models [18, 21] and particular applications [22, 23] show that the 'near-wall' formulations of Lam and Bremhorst [10] and Launder and Sharma [6] are the most suitable ones. These proposals use the same set of empirical constants postulated by Launder and Spalding [1], but Launder and Sharma employed the aforementioned ε decomposition and also the term E introduced previously by Jones and Launder [2, 3]. Those two near-wall formulations, together with the pioneering one of Jones and Launder [3], have been chosen for comparison purposes.

The boundary condition for ε at the wall proposed by Lam and Bremhorst [10]

$$\varepsilon_w = \nu \left[\frac{\partial^2 k}{\partial y^2}\right]_{\text{wall}} \tag{6}$$

has not been applied in the present work. Experimental evidence [13, 18, 24] supports the adoption of

$$\left[\frac{\partial \varepsilon}{\partial y}\right]_{\text{wall}} = 0 \tag{7}$$

as suggested by Patel *et al.* [18]. In addition, equation (7) has the advantage of not involving the turbulent kinetic energy.

Modelling

Predictions of transfer processes in duct flows obtained from previous k–ε models deviate from heat and/or mass transfer experimental data in situations where diffusion near the wall controls the transfer process, i.e. when $Pr \gg 1$. The same occurs whenever the mixing length equation of Nikuradse–Van Driest [25] is applied, except when used in conjunction with an unrealistic turbulent Prandtl number profile, function of the Prandtl number [26]. To overcome this drawback a modification of the Van Driest equation was proposed [20], which affects only the region $y^+ < 5$, that can be successfully applied with a constant $Pr_t \approx 0.9$. Using this approach, it was shown that there is a ν_t profile near the wall that yields accurate momentum transfer predictions as well as a α_t profile in accordance with experimental data, over a wide range of Pr. In the present work, this ν_t profile for $y^+ < 100$ and published k and ε data [27] have been used to elucidate the best form for the damping functions f_μ and f_1. It is convenient, however, to establish first the function f_2.

The majority of formulations included in Table 1 use for f_2 the proposal of Jones and Launder [2, 3]

$$f_2 = 1 - 0.3 \exp(-R_t^2) \tag{8}$$

which takes the value 0.7 at the wall. In the present study both the adoption of a model similar to the one proposed by Lam and Bremhorst [10], which requires $f_2 = 0$ at the wall because it does not include ϕ and E terms, and the implementation of boundary condition (7) instead of (6), have been accomplished with a simple modification of equation (8)

$$f_2 = 1 - (0.3/D) \exp(-R_t^2);$$
$$D = 1 - 0.7 \exp(-R_k). \tag{9}$$

This equation yields the same f_2 values as in equation (8) far from the wall and matches the required zero value at the wall.

Lam and Bremhorst [10] suggested that the damping function f_μ has to depend on the dimensionless numbers R_k and R_t. Hence, they proposed for f_μ

$$f_\mu = [1 - \exp(-0.0165 R_k)]^2 [1 + (20.5/R_t)]. \tag{10}$$

In the present work, equation (10) has been modified

$$f_\mu = [1 - \exp(-a R_k)]^2 [1 + (b/R_t) \exp(-c R_k)] \tag{11}$$

to obtain an appropriate near-wall ν_t profile just by adjusting the values of the constants and by introducing a damping factor to ensure an adequate transition of f_μ to unity in the fully turbulent region, far from the wall ($y^+ > 100$).

The remaining damping function f_1 has been modelled as

$$f_1 = 1 + \left(\frac{d}{f_\mu}\right)^2. \tag{12}$$

Equation (12), as suggested by Lam and Bremhorst [10], was found to perform better than the f_1 function adopted by these authors, which only differs from equation (12) in the value of the exponent (see Table 1).

All parameters and constants appearing in the damping functions f_μ and f_1 defined by equations (11) and (12) have been optimized so that the appropriate ν_t, or α_t with $Pr_t = 0.9$, profile is matched and, with the constants of equations (2)–(4) given in Table 1, the best pair of k and ε profiles are obtained. The optimal set of values is $a = 0.0066$, $b = 500$, $c = 0.0055$ and $d = 0.05$.

RESULTS AND DISCUSSION

Evaluation of the model

A turbulence model should at least accurately predict the mean velocity profile and the friction coefficient, which are important for engineering purposes. Figure 2 shows the values of C_f predicted by several k–ε models for turbulent pipe flow. Results obtained from Nikuradse's correlation [28] are also included. The proposals of Jones and Launder [3] and Launder and Sharma [6] over- and underpredict, respectively, the expected C_f values, whereas that of Lam and Bremhorst [10] slightly deviates from experimental data, with an average error of 5%. As a consequence, similar deviations can be expected when previous models are used for heat/mass transfer predictions at moderate Prandtl numbers.

The differences observed in Fig. 2 arise from the

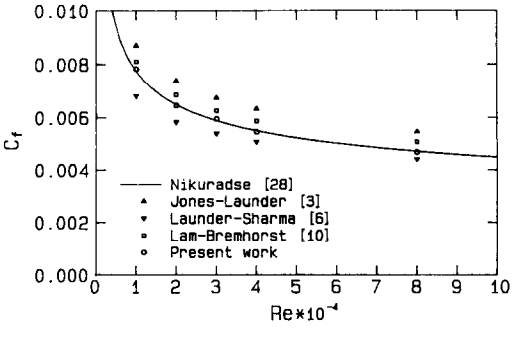

FIG. 2. Variation of skin friction coefficients with Reynolds number in pipe flow.

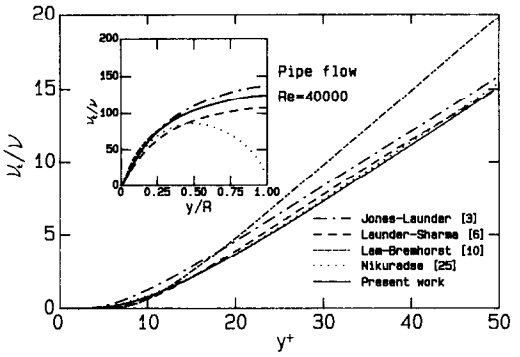

FIG. 3. Near-wall eddy viscosity profile in pipe flow.

predicted ν_t profiles, which are shown in Fig. 3 for the wall region. Since the steepest gradients occur in this region, the values in the core region do not influence significantly the overall momentum transport. It has been stated above that the ν_t profile obtained with the Nikuradse–Van Driest [25] mixing-length equation yields momentum predictions in accordance with experimental data for $y^+ \leqslant 100$. It should be remembered that any model yielding sufficiently low ν_t values in the viscous region ($y^+ < 5$) will correctly predict momentum transfer in this region, but not necessarily heat or mass transfer if $Pr > 1$ [20]. Thus, Fig. 3 reveals the origin of the discrepancies observed in Fig. 2. In the region $y^+ < 15$, all previous proposals referred to in this work for comparison purposes predict ν_t values that differ from the Nikuradse–Van Driest profile. Beyond this point, $y^+ > 15$, the Lam and Bremhorst [10] model has to overpredict ν_t in order to compensate the low near-wall predictions and to yield the C_f values shown in Fig. 2. The Jones and Launder formulation [3] gives high predictions for ν_t in the whole wall region, and so are those for C_f. The model of Launder and Sharma [6], although it yields ν_t values closer to the Nikuradse–Van Driest profile [25] for $y^+ > 15$, clearly underpredicts closer to the wall and, consequently, C_f is poorly estimated.

It has been shown that an eddy viscosity model which is able to reproduce the Nikuradse–Van Driest turbulent viscosity profile near the wall, will correctly predict momentum transfer. This objective has been reached in this work, as shown in Fig. 3. Figures 2 and 3 show that a good agreement for ν_t and C_f is obtained when the damping functions given by equations (9), (11) and (12) are introduced in the governing equations. The effect of the damping functions vanishes at the core region. This explains why in the inset of Fig. 3 the ν_t profile of Lam and Bremhorst [10] and present predictions coincide away from the wall. Such behaviour could be expected since both models are derived from the general form of the high Reynolds number formulation given by Launder and Spalding [1], in which all damping functions are taken as unity in the core region. It should be noted that the Nikuradse–Van Driest profile goes to zero at $y/R = 1$

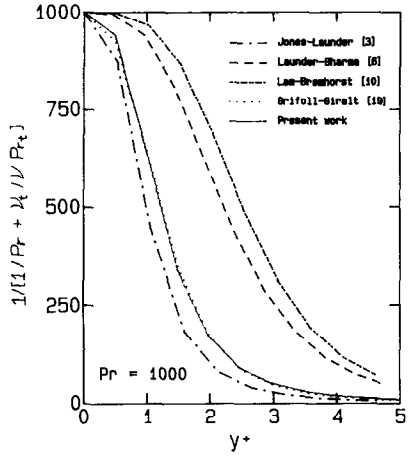

FIG. 4. Combined Prandtl number profile near the wall.

because it is generated by an algebraic equation defined to be used in a zero-equation model.

The α_t profile very close to the wall predicted in ref. [20] is accurately reproduced by the present formulation, as shown in Fig. 4. In this figure the inverse of the combined dimensionless diffusion coefficient $(1/Pr+\nu_t/(\nu\, Pr_t))$ is presented as a function of y^+ for $Pr = 1000$. This coefficient is obtained when the conservation equation (5) is normalized with respect to the friction velocity u_* and the length scale ν/u_*

$$U^+\frac{\partial T}{\partial x^+} = \frac{\partial}{\partial y^+}\left[\left(\frac{1}{Pr}+\frac{\nu_t}{\nu\, Pr_t}\right)\frac{\partial T}{\partial y^+}\right]. \qquad (13)$$

Note that the inverse of the dimensionless diffusion coefficient in equation (13) tends to the value of the Prandtl number as the wall is approached. In Fig. 4, Lam and Bremhorst [10] and Launder and Sharma [6] give too low ν_t values and, thus, too high combined Prandtl numbers to predict heat transfer phenomena properly, while the inverse is true for Jones and Launder [3]. These differences already indicate how predictions obtained from these three k–ε formulations may deviate from experimental heat transfer rates.

Heat transfer

Heat transfer calculations performed with present and previous k–ε equations, as well as with the zero-equation model proposed in ref. [20], are presented in Figs. 5–7 for various Prandtl numbers. All results presented in these figures correspond to numerical simulations of fully developed turbulent pipe flow.

Figure 5 shows the variation of the Nusselt number with the Prandtl number for $Re = 40\,000$. The empirical correlation obtained by Berger and Hau [29] from a large number of experimental data has also been included for comparison purposes. As can be seen, all previous k–ε models deviate from experimental data, with discrepancies increasing with Prandtl number. Some of them already deviate at $Pr = 1$, in the same way as C_f values do in Fig. 1, as expected. The best of

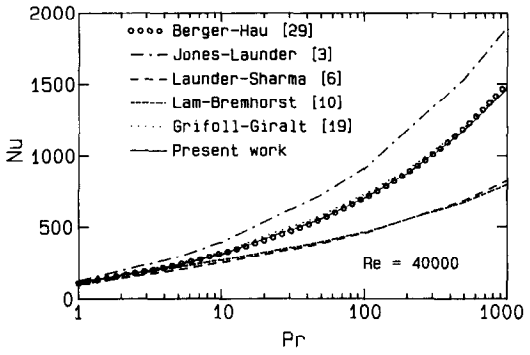

FIG. 5. Variation of the Nusselt number with Prandtl number at $Re = 40\,000$.

the previous k–ε models, from the point of view of heat transfer, is that of Jones and Launder [3], although it predicts Nusselt numbers 25% higher than experimental values at $Pr = 1000$. At this high Prandtl number, both Launder and Sharma [6] and Lam and Bremhorst [10] clearly underpredict the experimental data of Berger and Hau [29] by almost 50%. Only the present and the algebraic model given in ref. [20] are capable of matching the experimental trend over the range $1 < Pr < 1000$. Note that Grifoll and Giralt [20] assumed the value of 0.85 for the turbulent Prandtl number. When this Pr_t is used, their results differ by less than 2% at $Pr = 1000$ and by less than 3% at $Pr = 1$ from their predicted Nusselt numbers with $Pr_t = 0.9$.

Predicted dimensionless temperature profiles for $Pr = 0.7$ are compared with experimental data [30] in Fig. 6. It has to be noted that temperatures are normalized with respect to the heat flow rate, heat capacity and friction velocity, so that Reynolds number independence is attained. It is not surprising that Jones and Launder [3] and Launder and Sharma [6] clearly under- and overpredict, respectively, the experimental profile of Fig. 6 in the buffer and fully turbulent regions, due to the too high $\nu_t(\alpha_t)$ profile of the former and too low of the latter (see Fig. 3). The temperature predictions of Lam and Bremhorst [10], also shown in Fig. 6, are related with the behaviour of ν_t observed in Fig. 3. In this case ν_t values are very low for $y^+ < 10$ and excessively large beyond this

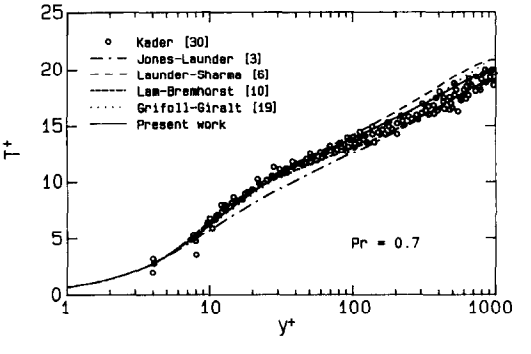

FIG. 6. Dimensionless temperature profile at $Pr = 0.7$.

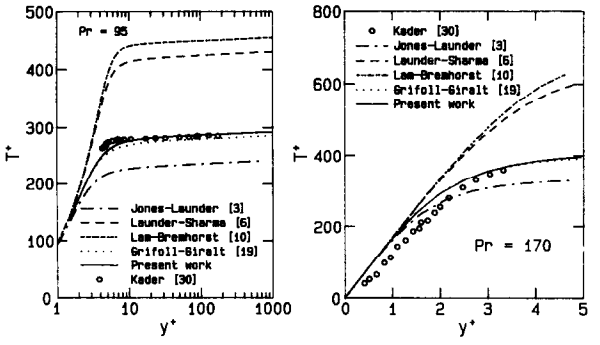

FIG. 7. Dimensionless temperature profiles: (a) $Pr = 95$; (b) $Pr = 170$.

point. Even though these opposite effects seem to compensate each other to some extent when integral properties, such as the friction coefficient (Fig. 2) or the temperature profile at moderate Prandtl numbers are calculated, it may be concluded that the Lam and Bremhorst proposal has to fail in predicting temperature profiles at higher Prandtl numbers because computed ν_t values are rather inadequate over the whole domain. On the other hand, present predictions reproduce accurately experimental data, showing only a slight negative deviation in the region $10 < y^+ < 30$. This agreement confirms once again the validity of the model developed in this work to obtain an appropriate eddy viscosity profile. The fact that present predictions fit experimental data even better than those of the zero-equation model suggests that this objective has been fully achieved.

The tendencies observed in Fig. 6 appear still more clearly in Figs. 7(a) and (b), where two dimensionless temperature profiles are presented for higher Prandtl numbers ($Pr = 95$ and 170). The results included in these figures keep a close relation with those presented in Fig. 4 because

$$Nu = Pr\,Re\frac{R^{+2}}{2\displaystyle\int_0^{R^+} T^+U^+r^+\,\mathrm{d}r^+}. \qquad (14)$$

In Fig. 7(b) the dimensionless distance from the wall is linearly scaled because only a very small region is covered. Present and previous models are compared again with the experimental data reported by Kader [30] in these figures. It is well known that at high Prandtl numbers, temperature gradients occur in the region very close to the wall ($y^+ < 5$) and so the whole profile is almost absolutely determined by temperature data in this region, as can be observed in both Figs. 7(a) and (b). Only the present k–ε model and the mixing length one of Grifoll and Giralt [20] are capable of describing the trend of experimental data. Launder and Sharma [6] and Lam and Bremhorst [10] profiles increase too fast, reaching too high T^+ values, while the opposite is true for Jones and Launder [3]. The discrepancy observed in Fig. 7(b) between all numerical predictions and experimental data in the linear near-wall zone of the dimensionless temperature profile may be attributed to the uncertainty of data caused by the experimental difficulties involved in measuring so close to the wall high Prandtl numbers. Even though the profile at $Pr = 95$ in Fig. 7(a) does not include data so close to the wall, it allows checking the location where the profiles change slope. This location is important because minimal deviations in this zone decisively affect the whole profile. Only the present k–ε model is capable of describing experimental values and trends. Also it is clear in Fig. 7(a) that the values of the dimensionless temperature obtained with the Lam and Bremhorst [10] and the Launder and Sharma [6] models largely deviate from experimental values, while those of Jones and Launder [3] deviate by 20%.

The above results indicate that whenever equation (5) is employed to solve the thermal field, heat transfer calculations at high Prandtl numbers can only be properly carried out if a suitable turbulent thermal conductivity profile is used. This profile has to yield a combined Prandtl number profile, for the very near-wall region, such as that of Grifoll and Giralt [20] presented in Fig. 4. Note that if a constant turbulent Prandtl number is assumed, the combined Prandtl number only depends on ν_t. Therefore, the profiles of α_t in Fig. 4 explain why previous models cannot describe the thermal field and fluxes at high Prandtl numbers, under a constant Pr_t assumption. In fact, some previous experimental evidence suggests that the turbulent Prandtl number does not remain constant very near the wall. Since there are important discrepancies between data from different workers [31], the constant Pr_t assumption seems, at present, correct enough. Furthermore, this assumption allows the simulation of heat transfer phenomena at solid boundaries over a wide range of Prandtl numbers.

Momentum transfer

One of the objectives of any turbulence model is to yield reasonably good predictions of turbulent mean properties such as the Reynolds shear stress, the turbulent kinetic energy and its dissipation rate. Figure 8 includes experimental and predicted Reynolds shear stress profiles for pipe flow at a Reynolds number of 40 000. The inset presents channel data at $Re = 7000$.

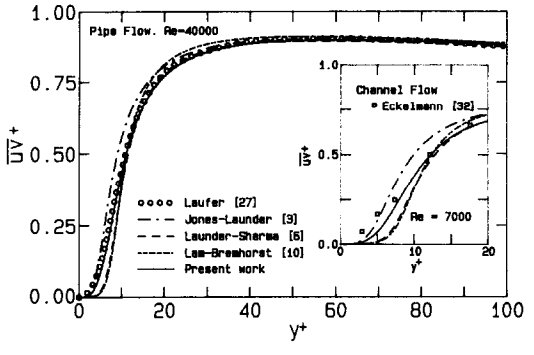

FIG. 8. Reynolds shear stress profile near the wall.

The significant differences observed between the numerical predictions obtained from previous k–ε models and the experimental data of Laufer [27] in the region $0 < y^+ < 50$ can be easily explained again looking back at Fig. 3. It is clear enough from the definition of the eddy viscosity that high ν_t values have to lead to high values of the Reynolds shear stress, and vice versa. This is what happens with the Jones and Launder [3] and Launder and Sharma [6] formulations in Fig. 8. Note that the Lam and Bremhorst $\overline{uv}^+$ curve crosses Laufer's experimental data [27] exactly at the same location that it does their predicted ν_t curve with the Nikuradse–Van Driest eddy viscosity profile in Fig. 3. Present predictions are in good agreement with experimental data, with slight deviations for $y^+ < 5$. The same tendencies are observed in the inset of Fig. 8, where the predicted turbulent shear stress profile for channel flow is compared with Eckelmann's [32] experimental data. Here a great similarity in tendencies with the combined Prandtl number profiles of Fig. 4 can be appreciated. The present proposal is the one that better reproduces the experimental trend, with deviations for $y^+ < 5$ probably due to the experimental difficulties involved in $\overline{uv}$ measurements so close to the wall.

An important indicator for testing turbulence models is their capability to predict experimental turbulent kinetic energy profiles. In Figs. 9(a) and (b) results are presented for pipe flow at $Re = 40\,000$. Comparison is established with previous and present near-wall k–ε formulations and with the experimental data of Laufer [27] and Schubauer [33]. The characteristic turbulent kinetic energy profile consists of a rapid increase from the zero value at the wall to a maximum peak located in the region $y^+ \approx 20$, followed by a progressive decay down to the centre of the pipe. This experimental trend, presented in Fig. 9(a) for the wall region ($y^+ \leqslant 100$), is reproduced, to some extent, by all k–ε formulations. The peak location is well predicted by all models, but Jones and Launder [3] and, especially, Launder and Sharma [6], underpredict the maximum value of the peak by 20 and 35%, respectively. Present predictions are approximately 25% higher than measurements, while the Lam and Bremhorst [10] model reproduces better the peak of the data of Laufer [27] and Schubauer [33]. The turbulent kinetic energy profile in the fully turbulent region is shown in Fig. 9(b). All models follow approximately the trend of experimental profiles, but fail to predict k values near the centre of the pipe. This could be explained by the intrinsic limitations of the two-equation models considered.

The pioneer work of Laufer [27] and of Schubauer [33] have been for years referenced by many authors for comparison purposes. However, more recent experimental data on turbulent channel flow indicate that the k peak for pipe flow should be higher than the peak values reported by Laufer and Schubauer. In Fig. 10(a) the experimental data of Clark [34] for fully developed turbulent channel flow at $Re = 25\,000$ is compared, for the wall region ($y^+ < 100$), with numerical predictions of previous and present k–ε proposals and with the large eddy simulation results obtained by Moin and Kim [35]. Although the Reynolds number is lower here than in Fig. 10(a), the dimensionless value of the experimental k peak is higher. All models underpredict the value of this peak, the present predictions being the closest. In fact, several authors [36, 37] have pointed out that the modelling of the k transport equation (3) is not adequate

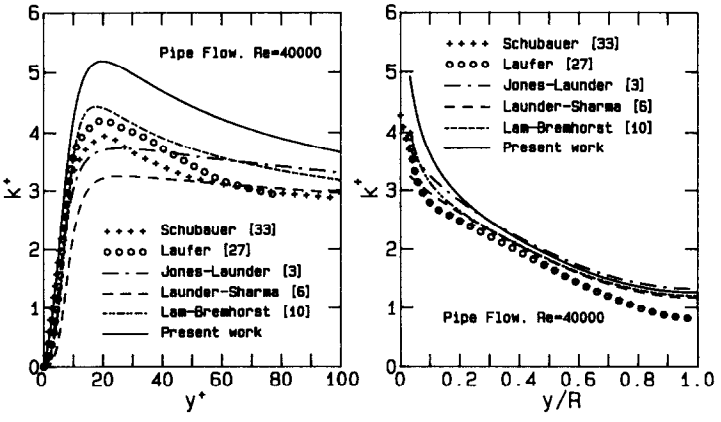

FIG. 9. Turbulent kinetic energy profiles for pipe flow at $Re = 40\,000$.

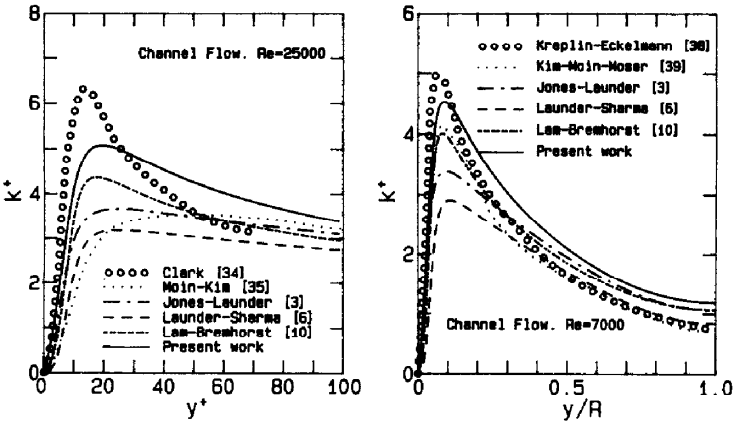

FIG. 10. Turbulent kinetic energy profiles for channel flow at $Re = 7000$ and 25 000.

for the near wall region and that the experimental value of the k peak cannot be reached whenever equation (3) is used.

In Fig. 10(a) it can also be observed that large eddy simulation [35] gives a poor description of the k profile, not only because the maximum value obtained for k is 50% lower than the experimental peak value, but also because the location of this maximum occurs too far from the wall, i.e. at $y^+ \approx 50$. This might demonstrate the influence of the Subgrid Scale Modelling involved in large eddy simulation of wall flows, but it could also be produced by a lack of accuracy caused by insufficient computational points. Previous and present k–ε proposals are compared in Fig. 10(b) with the experimental data of Kreplin and Eckelmann [38]. Also, the direct computer simulation results obtained by Kim *et al.* [39] for fully developed turbulent channel flow at $Re = 7000$ are included. In this figure the turbulent kinetic energy profile is represented for the whole domain, from the wall to the centre of the channel. The experimental value of the k peak is again higher than that of pipe flow data [27, 33]. All the k–ε proposals show the same behaviour observed in Figs. 9 and 10(a). The present formulation is the one which reproduces better the experimental k peak, while Jones and Launder [3] and Launder and Sharma [6] give very rough predictions. The peak location is correctly predicted by all k–ε formulations while predicted k values at the centre of the channel are higher for all k–ε models yielding best peak values. At this low Reynolds number the direct simulation predictions [39] show good agreement with experimental trends.

Finally, Fig. 11 compares measured and predicted distributions of the turbulent kinetic energy dissipation rate in the near-wall of fully developed pipe flow at $Re = 40\,000$. The experimental data of Laufer [27] and Schubauer [33], which are very similar and present a peak at $y^+ \approx 10$, are well reproduced by Launder and Sharma [6] and, less accurately, by the present proposal. Lam and Bremhorst's formulation notably underpredicts the ε peak. The behaviour of the Jones and Launder [3] profile is remarkable because while it reaches the maximum experimental value of ε, gives the peak at $y^+ \approx 5$. Note that all other models locate this peak at $y^+ \approx 10$. Another important difference between the different proposals is the ε value at the wall. This value apparently does not depend on the wall boundary condition employed for ε, since Jones and Launder [3] and Launder and Sharma [6], which use the same boundary condition (see Table 1), yield respectively the highest and lowest wall values. The experimental data [27, 33] suggest that the dimensionless value of ε_w is lower than 0.05. However, several authors [10, 17, 18] have indicated that the value of ε^+ at the wall could reach $0.05 \leqslant \varepsilon^+ \leqslant 0.1$, increasing with the Reynolds number. Thus, the value at the wall obtained by Launder and Sharma seems a little too low. The rest of the models yield wall values within the aforementioned range. All these results present a very different behaviour than the direct numerical simulation results reported by Mansour *et al.* [40], which give the maximum value of ε at the wall. As pointed out by these authors, however, it should be noted

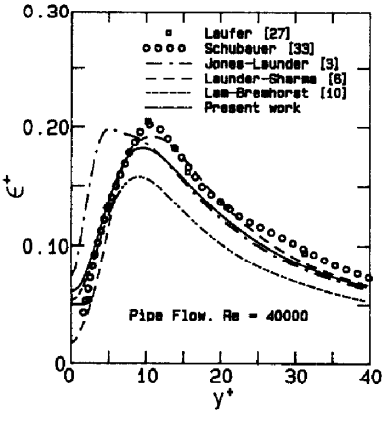

FIG. 11. Dissipation rate of turbulent kinetic energy near the wall in pipe flow at $Re = 40\,000$.

that there is a large difference between the Reynolds number of the simulation and that of Laufer's data. Nevertheless it remains the open question of whether or not the ε peak is located at the wall for moderate Re, i.e. if the trends shown by the direct simulation results for low Reynolds numbers are really in conflict with the available experimental data for higher Re.

CONCLUSIONS

A new set of damping functions for near-wall k–ε models has been obtained to predict heat and/or mass transfer processes at high Prandtl numbers since all previous two-equation formulations fail at even more moderate conditions. In order to establish the validity of the present and previous models, a numerical simulation of fully developed pipe and channel flow has been performed. Heat transfer rates and temperature profiles are accurately predicted by the present formulation with a maximum error of about 6% within the range $1 \leqslant Pr \leqslant 1000$ and $10^4 \leqslant Re \leqslant 10^5$, assuming a constant $Pr_t = 0.9$. The present formulation also predicts turbulent mean properties such as the mean velocity, friction coefficients, turbulent transport terms, turbulent kinetic energy and eddy viscosity at least with the same or even better reliability than previous near-wall k–ε models.

Acknowledgements—Financial assistance received from the CAICYT, project No. PB85-0446, is gratefully acknowledged. One of the authors (JH) was supported by a Spanish fellowship.

REFERENCES

1. B. E. Launder and D. B. Spalding, The numerical computation of turbulent flows, *Comp. Meth. Appl. Mech. Engng* **3,** 269–289 (1974).
2. W. P. Jones and B. E. Launder, The prediction of laminarization with a two-equation model of turbulence, *Int. J. Heat Mass Transfer* **15,** 301–314 (1972).
3. W. P. Jones and B. E. Launder, The calculation of low Reynolds number phenomena with a two-equation model of turbulence, *Int. J. Heat Mass Transfer* **16,** 1119–1130 (1973).
4. S. Hassid and M. Poreh, A turbulent energy dissipation model for flows with drag reduction, *J. Fluids Engng* **100,** 107–112 (1978).
5. G. H. Hoffman, Improved form of the low-Reynolds number k–ε turbulence model, *Physics Fluids* **18,** 309–312 (1975).
6. B. E. Launder and B. R. Sharma, Application of the energy-dissipation model of turbulence to the calculation of flow near a spinning disc, *Lett. Heat Mass Transfer* **1,** 131–138 (1974).
7. D. Dutoya and P. Michard, A program for calculating boundary layers along compressor and turbine blades. In *Numerical Methods in Heat Transfer*. Wiley, New York (1981).
8. K. Y. Chien, Predictions of channel and boundary-layer flows with a low-Reynolds-number turbulence model, *AIAA J.* **20,** 33–38 (1982).
9. W. C. Reynolds, Computation of turbulent flows, *Ann. Rev. Fluid Mech.* **8,** 183–208 (1976).
10. C. K. G. Lam and K. Bremhorst, A modified form of the k–ε model for predicting wall turbulence, *J. Fluids Engng* **103,** 456–460 (1981).
11. Y. Nagano and M. Hishida, Improved form of the k–ε model for wall turbulent shear flows, *J. Fluids Engng* **109,** 156–160 (1987).
12. C. G. Speziale, On nonlinear k–l and k–ε models of turbulence, *J. Fluid Mech.* **178,** 459–475 (1987).
13. K. Hanjalic and B. E. Launder, A Reynolds stress model of turbulence and its application to thin shear flows, *J. Fluid Mech.* **52,** 609 (1972).
14. P. Bradshaw, Turbulent secondary flows, *Ann. Rev. Fluid Mech.* **19,** 53–74 (1987).
15. C. Hah and B. Lakshminarayana, Numerical analysis of turbulent wakes of turbomachinery rotor blades, *J. Fluid Engng* **102,** 462–472 (1980).
16. J. G. Marvin, Turbulence modeling for computational aerodynamics, *AIAA J.* **21,** 941–955 (1983).
17. J. O. Hinze, *Turbulence*. McGraw-Hill, New York (1975).
18. V. C. Patel, W. Rodi and G. Scheuerer, Turbulence models for near-wall and low Reynolds number flows: a review, *AIAA J.* **25,** 1308–1319 (1984).
19. S. P. Vanka, Block-implicit calculation of steady turbulent recirculating flows, *Int. J. Heat Mass Transfer* **28,** 2093–2103 (1985).
20. J. Grifoll and F. Giralt, Mixing length equation for high Schmidt number mass transfer at solid boundaries, *Can. J. Chem. Engng* **65,** 18–22 (1987).
21. A. Pollard and R. Martinazzi, A comparative study of eleven models of turbulence, 6th Symp. on Turbulent Shear Flows, Toulouse, pp. (17-9-1)–(17-9-5) (1987).
22. W. Rodi and G. Scheurer, Scrutinizing the k–ε turbulence model under adverse pressure gradient conditions, *J. Fluids Engng* **108,** 174–179 (1986).
23. M. A. Cotton and J. D. Jackson, Calculation of turbulent mixed convection in a vertical tube using a low-Reynolds-number k–ε turbulence model, 6th Symp. on Turbulent Shear Flows, Toulouse, pp. (9-6-1)–(9-6-6) (1987).
24. K. Hanjalic and B. E. Launder, Contributions towards a Reynolds-stress closure for low-Reynolds number turbulence, *J. Fluid Mech.* **74,** 593–610 (1976).
25. E. R. Van Driest, On turbulent flow near a wall, *J. Aero. Sci.* **23,** 1007–1011 (1956).
26. A. Malhotra and S. S. Kang, Turbulent Prandtl number in circular pipes, *Int. J. Heat Mass Transfer* **27,** 2158 (1984).
27. J. Laufer, The structure of turbulence in fully developed pipe flow, NACA Technical Note 2954 (1953).
28. H. Schlichting, *Boundary Layer Theory*. McGraw-Hill, New York (1979).
29. F. P. Berger and K.-F. F.-L. Hau, Mass transfer in turbulent pipe flow measured by the electrochemical method, *Int. J. Heat Mass Transfer* **20,** 1185–1194 (1977).
30. B. A. Kader, Temperature and concentration profiles in fully turbulent boundary layers, *Int. J. Heat Mass Transfer* **24,** 1541–1544 (1981).
31. A. L. Snijders, A. M. Koppius and C. Nieuwvelt, An experimental determination of the turbulent Prandtl number in the inner boundary layer for air flow over a flat plate, *Int. J. Heat Mass Transfer* **26,** 425–431 (1983).
32. H. Eckelmann, The structure of the viscous sublayer and the adjacent wall region in a turbulent channel flow, *J. Fluid Mech.* **65,** 439–459 (1974).
33. G. B. Schubauer, Turbulent processes as observed in boundary layer and pipe, *J. Appl. Phys.* **25,** 188–196 (1954).
34. J. A. Clark, A study of incompressible turbulent boundary layers in channel flow, *ASME Trans., J. Basic Engng* **90,** 455–466 (1968).
35. P. Moin and J. Kim, Numerical investigation of turbulent channel flow, *J. Fluid Mech.* **118,** 341–377 (1982).
36. C. G. Speziale, Modeling the pressure gradient–velocity correlation of turbulence, *Physics Fluids* **28,** 69–71 (1985).

37. T. H. Shih and L. P. Chang, A near wall k–ε turbulence model, Personal Report (1987).
38. H. P. Kreplin and H. Eckelmann, Behaviour of the three fluctuating velocity components in the wall region of a turbulent channel flow, *Physics Fluids* **22,** 1233–1239 (1979).
39. J. Kim, P. Moin and R. Moser, Turbulence statistics in fully developed channel flow at low Reynolds number, *J. Fluid Mech.* **177,** 133–166 (1987).
40. N. N. Mansour, J. Kim and P. Moin, Reynolds-stress and dissipation-rate budgets in a turbulent channel flow, *J. Fluid Mech.* **194,** 15–45 (1988).

UNE FORMULATION k–ε PROCHE DE LA PAROI POUR LE TRANSFERT THERMIQUE A GRAND NOMBRE DE PRANDTL

Résumé—On propose une forme de modèle de turbulence k–ε près de la paroi. Les fonctions d'amortissement pris en compte pour les effets visqueux à faible nombre de Reynolds sont modifiées pour introduire une viscosité turbulente qui prédit correctement les flux de chaleur dans un large domaine de nombre de Prandtl, en utilisant un nombre de Prandtl turbulent constant $Pr_t = 0{,}9$. Ces modifications conduisent à améliorer les prédictions de flux pariétaux et elles donnent aussi une meilleure description des profils de vitesse moyenne et de température aussi bien que des propriétés moyennes de turbulence.

EIN WANDNAHES k–ε-MODELL FÜR WÄRMEÜBERTRAGUNG BEI HOHER PRANDTL-ZAHL

Zusammenfassung—Es wird eine verbesserte Formulierung des sogenannten "wandnahen" k–ε-Turbulenzmodells vorgeschlagen. Die Dämpfungsfunktionen zur Berücksichtigung der Reibungseffekte bei kleinen Reynolds-Zahlen werden modifiziert. Damit ergibt sich eine turbulente Viskosität, mit deren Hilfe der Wärmeübergang in einem weiten Bereich der Prandtl-Zahl erfolgreich berechnet werden kann. Als turbulente Prandtl-Zahl wird dabei der konstante Wert $Pr_t = 0{,}9$ verwendet. Diese Modifikationen sollten ursprünglich die Berechnung der Wandstromdichten verbessern, sie liefern jedoch zusätzlich eine bessere Beschreibung der mittleren Geschwindigkeits- und Temperaturprofile wie auch der mittleren turbulenten Eigenschaften.

ФОРМУЛИРОВКА ДВУХПАРАМЕТРИЧЕСКОЙ k–ε МОДЕЛИ ТУРБУЛЕНТНОСТИ В ПРИСТЕННОЙ ОБЛАСТИ ПРИ ТЕПЛОПЕРЕНОСЕ С ВЫСОКИМИ ЧИСЛАМИ ПРАНДТЛЯ

Аннотация—Предложен усовершенствованный вид двухпараметрической k–ε модели турбулентности в пристенной области. Функции затухания, учитывающие эффекты вязкости при низких числах Рейнольдса, с использованием постоянного турбулентного числа Прандтля $Pr_t = 0{,}9$ модифицируются для определения турбулентной вязкости, которая позволяет правильно предсказывать скорости теплопереноса в широком диапазоне изменений числа Прандтля. Предложенные модификации позволяют повысить точность определения не только пристенных потоков, но и профилей средних скоростей и температур и средних параметров турбулентности.